Journal of Polymers and the Environment (2022) 30:5239–5251
https://doi.org/10.1007/s10924-022-02587-y

ORIGINAL PAPER

Preparation of Photochromic and Photoluminescent Nonwoven Fibrous Mat from Recycled Polyester Waste

Hend Ahmed[1] · Meram S. Abdelrahman[1] · Naser G. Al-Balakocy[2] · Zhen Wen[3] · Tawfik A. Khattab[1]

Accepted: 7 September 2022 / Published online: 29 September 2022

Abstract

Photochromic and photoluminescent clothes can be described as smart textiles that alter their color and emission spectra upon exposure to a light stimulus. Recycled nonwoven polyester fabrics screen-printed with rare-earth strontium aluminate nanoparticles were developed to introduce photochromic and photoluminescent properties. Both spinning and preparation of nonwoven fibrous mat was performed industrially starting from recycled polyester waste. Aqueous-based phosphor-binder nanocomposites containing different concentrations of inorganic phosphor with excellent thermal and photostability were applied directly onto nonwoven polyester fabrics. The screen-printing process produced a uniform photochromic and photoluminescent film onto the nonwoven polyester surface that showed strong green emission color (440 nm) under UV light even at lower phosphor concentrations (0.5 wt%) in the printing paste. The excitation wavelength of the printed nonwoven polyester samples was monitored at 382 nm. Long-persistent greenish-yellow phosphorescence was detected in the dark at higher phosphor concentrations. The morphological microscopic data of phosphor nanoparticles and printed nonwoven polyester fabrics were collected using various analytical methods. TEM analysis of phosphor nanoparticles designated diameters of 4–11 nm, whereas XRD analysis indicated a crystal size of 9 nm. The printed cloth exhibited a quick and reversible photochromic emission when exposed to ultraviolet light. The ultraviolet protection, antimicrobial and superhydrophobic properties were improved with increasing the pigment concentration in the printing paste. The static contact and slide angles improved in the ranges of 108.6°–132.6°, and 12°–7°, respectively. The effects of increasing the phosphor concentration in the printing paste on the comfort features and colorfastness were examined.

Keywords Nonwoven polyester fabric · Lanthanide-doped aluminate nanoparticles · Photochromism · Fluorescence · Long-persistent phosphorescence

Introduction

Smart fabrics has been defined as clothes that perceive and respond to ambient variables like temperature, pH, chemicals, magnetic field, light, solvent polarity, pressure, and electricity [1–3]. Wearable smart textiles can help regulate muscle vibrations during physical activity and even release chemicals that can regulate body temperature. They can alter their colors and show optical patterns such as images and even videos [4–7]. As a general rule of thumb, smart clothes must have three primary parts, including sensor, actuator, and controller. The classic textile manufacturing processes, including weaving, knitting, embroidery, finishing, coating and laminating, are often used in the production of smart clothing [8–10]. Digital components integrated in textiles can also provide the potential to transform, communicate and conduct energy, providing smart electronic textiles. It is possible for smart textiles that have sufficient responsiveness to boost their sensing ability [11]. For instance, a photochromic fabric changes its color once exposed to light [12]. A photochromic compound, in either solution or solid state, can change its color upon exposure to light and returns to its origin colorimetric state when the light stimulus is removed. Scientific attention has been paid to this unique color-changing technology, which can be used in various products like

✉ Tawfik A. Khattab
ta.khattab@nrc.sci.eg

[1] Dyeing, Printing and Auxiliaries Department, National Research Centre, Cairo 12622, Egypt

[2] Protenic and Manmade Fibers Department, National Research Centre, Cairo 12622, Egypt

[3] Institute of Functional Nano & Soft Materials (FUNSOM), Soochow University, Suzhou 215123, Jiangsu, China

sunglasses, optical switches, cosmetics, packaging, ophthalmic lenses, optical data storage, memory, displays, and sensors [13–15]. Using photochromic or fluorescent colorants enhances the visibility of various products such as traffic and road signs, and advertisements [16–20]. Imparting photochromism to textiles can provide inventive materials to achieve smart clothing able to block and sense harmful ultraviolet rays, and provide security prints for brand protection, fire brigades and policeman clothing, electronic displays, security barcodes, sport clothing, fashion garments, sensor systems, and attractive decorations [21–23]. It has been also possible to use the photochromic effect in military apparel to create light-induced camouflage [24]. The advantages of stimuli-responsive and protective clothing are their ease of washing and drying, extraordinarily high surface area, light weight, as well as enhanced elasticity, tensibility, and strength. In addition to their low cost and wide availability, various sensors can be easily integrated into protective clothing systems without requiring any changes to the manufacturing process [25]. Fabrics with photochromic properties could be made without having to compromise their comfort or ease of care. Thus, researchers have been challenged to design innovative smart textiles with fluorescence-driven photochromism [26].

Photochromic fabrics can be classified into two categories: fabrics that emit different colors once induced with visible light source, and photochromic fibers that emit different color upon exposed by UV rays [27]. Many fibers and/or textiles have been dyed using photochromic and photoluminescent organic dyes, such as spirooxazines, in order to make photochromic fibers and/or fabrics from various substrates such as cotton and polyester [28]. However, photochromic and photoluminescent organic dyes pose a number of disadvantages during the dyeing process, including degradation of dye molecules, weak interaction of the organic dye with fibers, and inhibition of photochromic activity due to matrix hardness [29]. The performance of photochromic and photoluminescent organic compounds can be improved by microencapsulation. Despite the increased stability of photochromic compounds achieved by microencapsulation, this procedure could have a detrimental effect on the fabric comfort properties [30–33]. Otherwise, photochromic fabrics could be made by screen-printing technology utilizing an aqueous binding agent enclosing photochromic and photoluminescent dyestuff, which avoids many dyeing disadvantages. It has been straightforward and inexpensive to use screen-printing to create prints [34]. Pigment printing tops the list of textile printing industry as it has been the oldest and most straightforward coating method. Pigment printing technology has been used for about 80% of printed textiles because of its apparent benefits, such as versatility [35]. In contrast to inorganic pigments, organic photochromic and photoluminescent colorants have a lower photostabilty and are more expensive. Due to the fact that the organic colorants based photochromic textiles are quickly fade due to extended exposure to repetitive washing, heat, perspiration, light, and rubbing, photochromic fabrics often have poor qualities that need to be enhanced to suit customer expectations [28–30]. Using a screen-printing approach, inorganic pigment phosphor may be immobilized onto a binder-thickener printing matrix before being incorporated into the fabric surface to create photochromic textiles with improved photochromic and photoluminescent capabilities, dye stability, and comfort properties [36]. Textile substrates could benefit greatly from photochromic and fluorescent qualities provided by strontium aluminate phosphors that preserve the original fabric/fiber features like appearance, handling, comfortability and stiffness. As of today there are a variety of long-lasting luminous materials that could be used as primary color emitters like Eu^{2+}/Dy^{3+} doped $CaMgSi_2O_6$ [37] and Eu^{2+}/Nd^{3+} doped $CaAl_2O_4$ [38] for bluish emission, Eu^{2+}/Dy^{3+} doped $SrAl_2O_4$ [39] and Mn^{2+} doped $MgAl_2O_4$ [40] for greenish emission, and $Eu^{2+}/Tm^{3+}/Ce^{3+}$ doped CaS [41] and $Eu^{3+}/Mg^{2+}/Ti^{4+}$ doped Y_2O_2S [42] for reddish emission. Using $SrAl_2O_4$: Eu^{2+}, Dy^{3+} as a long-lasting phosphor, it was shown to have outstanding chemical and photostability, better brightness, and longer persistence period. It is also harmless, radioactive-free, and recyclable [43–47]. A new approach to developing more effective and stable smart garments is to use inorganic pigment phosphor in aqueous binder to print high-tech textiles that can be tuned for specific photochromic and photoluminescent properties. This approach is cost-effective, and opens up new avenues for the production of more efficient and stable functional clothing. The screen-printing application of an aqueous binder containing strontium aluminate phosphor onto recycled nonwoven polyester fabrics to produce light-responsive color changeable textiles has not yet been described.

Experimental

Materials

Thickener alcoprint PTP and Binder additive were purchased from Dystar (Egypt). All raw materials utilized in the synthesis of rare-earth strontium aluminate were obtained from different commercial sources, including europium (III) oxide (Eu_2O_3; Merck), strontium (II) carbonate ($SrCO_3$; Aldrich), boric acid (H_3BO_3; Merck), aluminium (III) oxide (Al_2O_3; Merck), and dysprosium (III) oxide (Dy_2O_3; Aldrich).

Spinning Process of Recycled Polyester Waste

Recycled polyester chips were firstly dried at 140 °C before extrusion. The dry mix was placed in hoppers tanks. The

extrusion process was carried out on the spinning line located in MakaremTex Company, Abu-Rawash, Six-October City, Giza, Egypt. The melt was subjected to an extrusion process using an automatic pressure control booster pump. The extrusion process was carried out under constant rate, and then adjusted with geared pump. Screw extruder with length-to-diameter of 24 was employed to conduct the extrusion process at 300 psi using three static mixers. The extruder initial zone was adjusted at 200 °C, the second zone was adjusted at 220 °C, and the third one was set at 250 °C. A spin pack was applied for the multi-filament spinning yarns, and was coupled to mesh filtration screen. The spinneret round orifice had a diameter of 0.7 mm, and a length of 1.5 mm. The multi-filament yarn was cooled to ambient conditions, and treated with lubricant before drawing at a ratio up to 2. The final denier was monitored at 6–15.

Manufacturing of Polyester Nonwoven Fabrics

The provided polyester fibers from the previous pilot scale production have been used for the manufacturing of the corresponding nonwoven fabrics. This was carried out using mechanical needle punched process on the production Line of Egyptex Company in Six-October City, Giza, Egypt. The needle punch industry has been one of the most successful achievements in textile-related industrial processes for both synthetic and natural fibers. The needle punching process for nonwovens was developed by mechanical orientation and interlock of polyester fibers by carded web or spun bonded procedures. The nonwoven fabric depends on fibrous webs. The web properties determine the physical behavior of the product [48–50]. The web properties rely mainly on the web geometrical properties, which can be reported by the web formation mode. The web geometrical properties includes the degree of interfiber entanglements or engagements, fiber shape (curled, hooked or straight), the predominant fiber direction (random or oriented), and compaction (crimp or z-direction). The web properties were also affected by web weight, fiber length, fiber diameter, as well as the mechanical and chemical properties of the polymer. The forming web method was identified by the length of fiber. The web formation from Staple-Length Fibers depends on the carding process. On the other hand, the web forming method from short fibers depends on the papermaking technology. Although those technologies are still in use, new techniques have been presented in textile industry. For instance, the web is prepared from long virtually endless filaments directly from the polymer bulk, whereas fibers are prepared simultaneously.

Preparation of Phosphor Nanoparticles

The high-temperature solid-state synthetic procedure [51] was used to synthesize the strontium aluminate phosphor ($SrAl_2O_4$: Eu^{2+}, Dy^{3+}). The powder compounds, Eu_2O_3, Al_2O_3, $SrCO_3$, and Dy_2O_3, were admixed with 5% of H_3BO_3 according to a mole ratio of Dy:Eu:Al:Sr = 0.01:0.02:1:2. The admixture was dispersed in ethanol (100 mL), and exposed to ultrasonic at 35 kHz for 20 min. It was dried at 90 °C over 22 h, pulverized in a ball milling system for two hours, and sintered at 1300 °C (3 h). The provided powder was then milled and sieved using Triple Roll Mill ES80 to afford Eu^{2+}, Dy^{3+} activated strontium aluminate phosphor microparticles (11–23 μm). To obtain the pigment nanoscale particles, the provided microscale fine particles (10 g) was placed in a ball milling vial mounted on a vibrating disc according to the top–down method [52]. Another ball milling made of silicon carbide (SiC) was exposed to repetitive collisions for 24 h with the pigment micropowder in the vial and the vibration disc to provide the phosphor nanoscale particles. The morphology of the phosphor nanoparticles was verified by transmission electron microscopy (TEM) and X-ray diffraction (XRD).

Preparation of Photoluminescent Nonwoven Polyester Fabrics

A high-speed mixer was used for 10 min to enable the synthetic thickening alcoprint PTP (2%; w/v) in distilled water to reach full viscosity. A mixture of NH_4OH (0.2%; w/w), diammonium phosphate (0.2%; w/w), and a binding agent (15%; w/w) was combined with alcoprint PTP thickener (84.6%; w/w) to create the printing stock paste. A high-shear mixer was used to stir the phosphor pigment at different ratios, including zero, 0.1, 0.5, 1, 3, 5, 7, 9, 11, 13, and 15% (w/w) for 15 min. The phosphor nanoparticles must be effectively dispersed in the printing paste without aggregation in order to form transparent pigment-binder composite layer onto polyester surface. Printing pastes are thickened with a little quantity of thickener when the viscosity of the printing paste drops below 21,000 cps at a shear rate of 2.18. The flat print screen was used to apply all printing pastes onto nonwoven polyester textiles. After drying for 30 min at room temperature, an automated thermo-static oven (Werner Mathis; Switzerland) thermally fixed the finished textiles for 4 min. The provided printed fabrics were subjected to washing with water (50 °C), washing with tap water, and then air-dried. Depending on the phosphor concentration, the screen-printed nonwoven polyester fabrics (NPF) were represented by symbols from NPF_0 to NPF_{10}, respectively. The morphological microscopic data of the printed nonwoven polyester fabrics were collected by energy-dispersive X-ray analyzer (EDXA), scanning electron microscopy (SEM), Fourier-transform infrared spectroscopy (FT-IR), and X-ray fluorescence (XRF).

Characterization and Methods

Morphological Features

The morphological analysis and chemical composition were handled by Quanta FEG250 (SEM; Czech Republic) paired to EDXA (TEAM Model). In addition to EDXA, sequential AXIOS XRF was employed to report the elemental contents of the printed polyester substrates. XRD analysis of the phosphor nanoparticles was examined by X-ray diffractometer (Bruker Advance D-8; copper radiation (Kα); Germany). The crystallite size was determined by Scherrer's equations [5, 44]. TEM (JEOL1230; Japan) was utilized to study the morphology of the phosphor particles that were previously suspended in distilled water, and homogenized (35 kHz) for 30 min. FT-IR spectral analysis was used in the ATR mode using Nexus 670 (Thermo Nicolet, Madison, WI, USA).

Luminescence Spectra

JASCO FP-8300 spectrofluorometer (JASCO; Japan) was utilized to analyze the emission and excitation spectra of the printed polyester substrates at room temperature. Phosphorescence accessories were applied to measure lifetime spectra. The ultraviolet supply is Xenon Arc (150 W) with slit bandwidth of 5 nm. All emission spectra were collected under the same geometrical circumstances. The instrument introduces corrected excitation spectral analysis, and the emission spectral analysis was corrected for the emission monochromator and photomultiplier responsiveness. The ultraviolet- irradiation was provided by an ultraviolet light supply (365 nm; 6 W).

Resistance to Fatigue

According to previously reported procedures [53], the technical performance and colorimetric changes of the printed polyester samples were examined. NPF_8 was exposed to ultraviolet irradiation for 4 min, and placed in a darkened box for 60 min. The irradiation/darkening cycle was performed several times, while recording the emission spectra.

Colorimetric Properties

Using the three-dimensional CIE Lab coordinate system (L*, a*, and b*) was used to report the colorimetric values [46, 47]. An ultraviolet lamp (λ_{max} = 365 nm; 6 W) was employed to irradiate the fabric for 4 min. The colorimetric measurements were reported before and directly after irradiation. The high reflectance approach was employed to gauge the colorimetric strength (*K/S*) of the printed samples. Photographic images of the phosphor-containing polyester fabric (NPF_8) were captured by A710IS Canon digital camera.

Colorfastness Assessment

The colorfastness properties of the printed nonwoven polyester fabrics were determined according to previously reported standard procedures, including ISO:105:X12 (1987) for crocking, ISO:105:B02 (1988) for light, ISO:105:E04 (1989) for perspiration, and ISO:105:C02 (1989) for washing [54, 55].

Comfort Properties

Textest FX 3300 (ASTM D737 standard method) was used to measure the air permeability of the screen-printed nonwoven polyester fabrics at 100 Pa [56]. Shirley Stiffness tool was employed to record stiffness under British standard 3356(1961) standardized method [57].

Hydrophobic Properties

Both contact and slide angles were examined by Data physics OCA15EC (Germany) under ASTM D7334 standard method [58].

Assessment of UV Protection

According to previously reported procedures [59], the printed polyesters were inspected by recording the Ultraviolet Protection Factor (UPF) to explore their UV protection. The ultraviolet/visible spectrophotometer system (AATCC 183:2010 UVA Transmittance) was used to calculate the UPF of the sun-protective samples described by AS:NZS 4399(1996).

Antimicrobial Features

The antimicrobial properties of printed samples were studied against *C. albican, S. aureus* and *E. coli*. The antimicrobial tests were conducted quantitatively under AATCC 100:1999 procedure [60].

Results and Discussion

Characterization of Printed Polyesters

Organic photochromic dyes undergo a structural change as a result of their photophysical transition, which has a detrimental influence on their photochromic properties.

Thus, steric hindrance has been a common problem for organic photochromic dyes when they are enclosed in printed films, which results in hampered performance of their photochromic activity [28, 29]. With poor photostability and limited use in outdoor conditions or under intense UV light, continuous UV exposure to organic photochromic molecules could cause deterioration and progressive reduction in their photochromic reaction [28–30]. Strontium aluminate pigments doped with divalent europium have previously been shown to be highly photostable under UV light, with increased fatigue resistance as well as rapid coloration/decoloration transitions. Thus, strontium aluminate phosphors have been used recently in countless products like switches, lights, smart inks, glow in the dark items, smart windows, luminous decorations, smart packaging, guiding signs, and safety markers [43–45]. The morphology and size of the rare-earth activated strontium aluminate nanoscale particles were examined by TEM images to indicate spherical structure with diameters of 4–11 nm as shown in Fig. 1.

XRD spectra of phosphor nanoparticles were analyzed. The phosphor diffraction signals were identical to the pure monoclinic phase of $SrAl_2O_4$. The absence of other signals indicates full integration of dopants (Eu^{2+} and Dy^{3+}) into low temperature monoclinic phase of $SrAl_2O_4$ crystal lattice [44]. Using Scherrer's equation [5], the phosphor crystal size was detected at 9 nm, which is well-matched with the particle size detected by TEM. The morphologies of the screen-printed nonwoven polyester fabrics were examined by SEM, EDXA, XRF and FTIR. The physical properties of the fabric fibrous structure were not affected after printing. However, the SEM images of the screen-printed nonwoven polyester surface displayed clusters of lanthanide-doped strontium aluminate nanoparticles as presented in Fig. 2. The elemental compositions of both blank and screen-printed nonwoven polyester fabrics were studied by EDXA (Fig. 3). The elemental contents at three points on the nonwoven polyester surface are shown in Table 1. The chemical compositions of the colored nonwoven polyester fabrics were quite similar

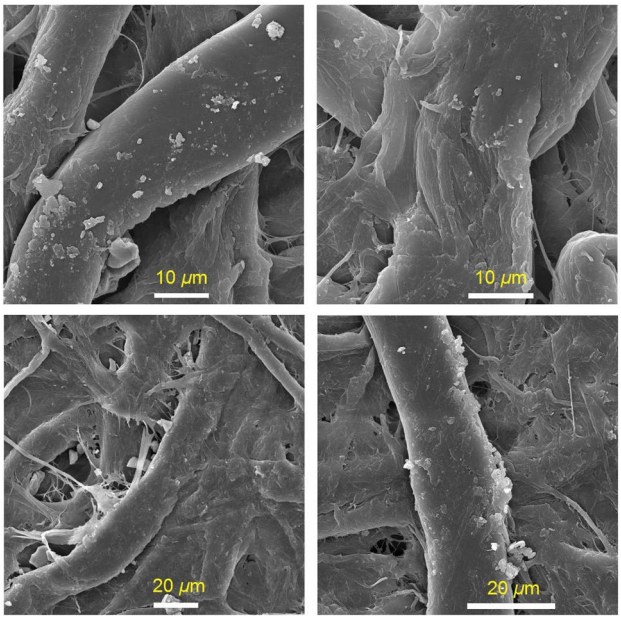

Fig. 2 SEM images of NPF_8 at various magnifications

at the three inspected points, confirming homogeneous phosphor distribution on the nonwoven polyester surface. The mapping of elements on fabrics was also examined to confirm a homogeneous distribution of $SrAl_2O_4$: Eu^{2+} Dy^{3+} (Fig. 4).

In the polyethylene terephthalate polymer that makes up the nonwoven polyester fabric, carbon (C) and oxygen (O) are the main constituents detected by EDX. The use of lanthanide-doped strontium aluminium oxide at low concentrations was the cause for the recognition of Al, Eu, Dy, and Sr. The elemental compositions of the screen-printed polyesters were reported by XRF as shown in Table 2. EDX is a precise method for the determination of elemental contents at low concentrations. XRF has a detection limit of 10 ppm [61]. XRF affords incomplete elemental detection,

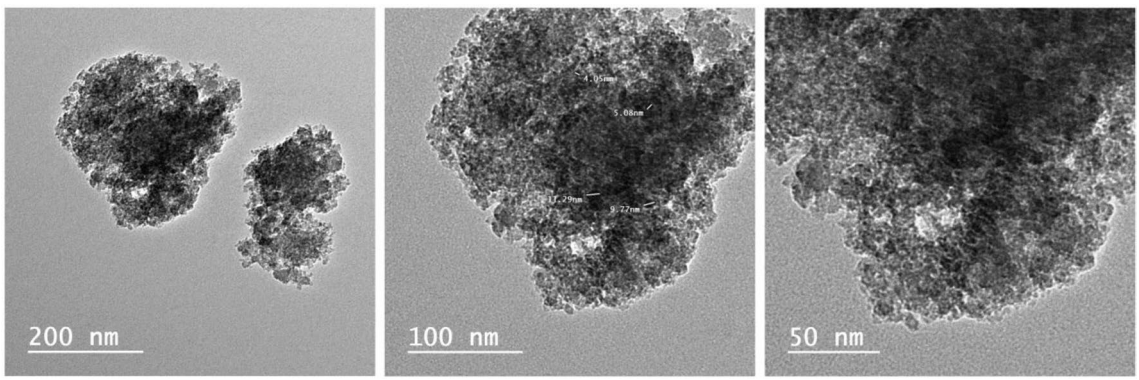

Fig. 1 TEM micrographs of lanthanide-doped aluminate nanoparticles

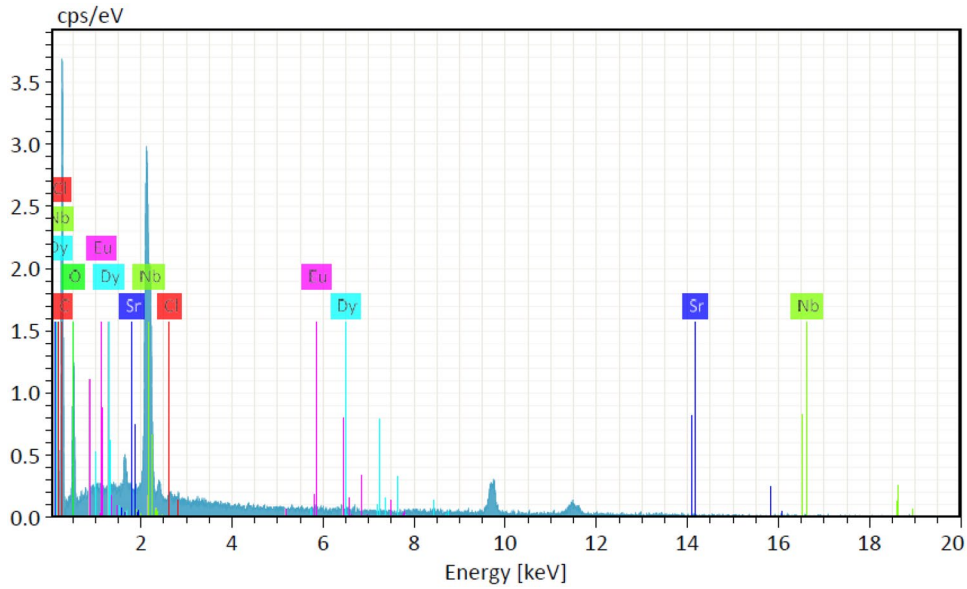

Fig. 3 EDX diagram of NPF_8.

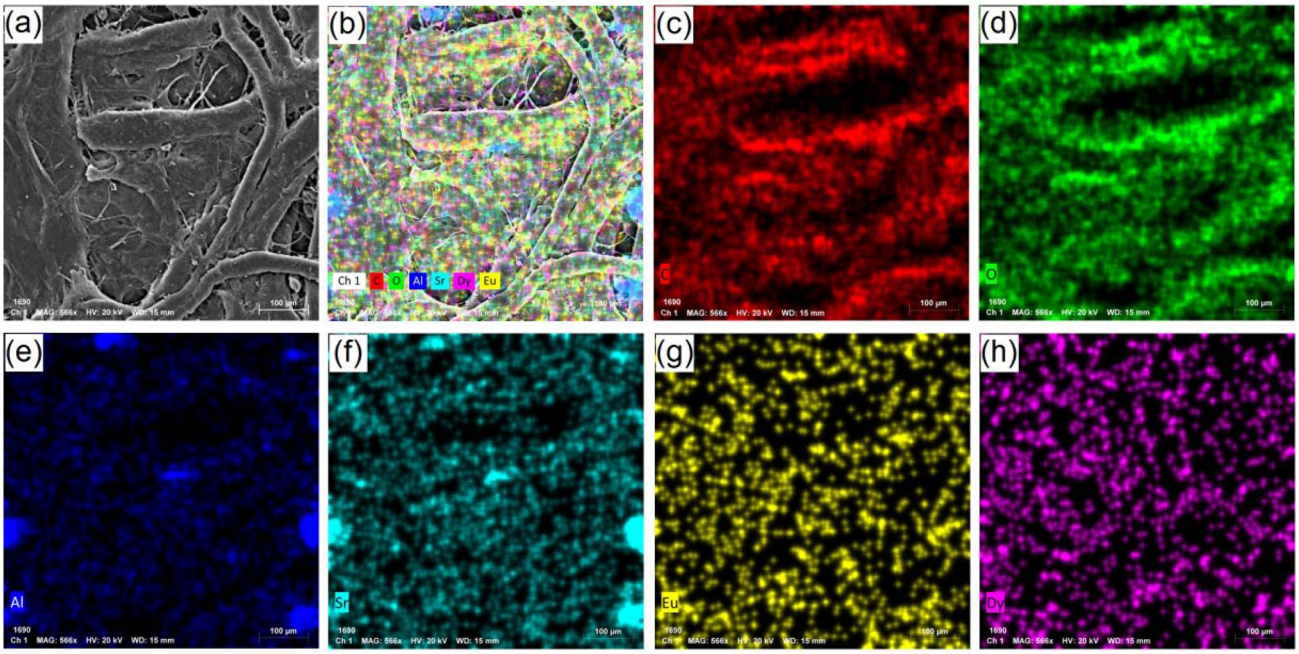

Fig. 4 Elemental mapping of NPF_8.

identifying only strontium and aluminium because Dy and Eu are present in very low concentrations less than 10 mg/kg on the treated cloth surface. Thus, XRF was incapable to recognize Dy and Eu in NPF_1, NPF_2, NPF_3, and NPF_4. The molar ratios applied to synthesize both pigment and screen-printing paste were compatible with those identified by EDXA and XRF on the screen-printed polyesters.

The functional substituents on the surface of the non-woven polyester fabrics were inspected by FTIR spectra as depicted in Fig. 5. The aliphatic C–H stretch displayed an absorption band at 2961 cm^{-1}. The carbonyl stretch was attributed to the absorption band at 1707 cm^{-1} [62]. The symmetric tetrahedron lattice structures of Al–O and O–Al–O were proved by two bands at 431 and 719 cm^{-1}, respectively. The peak monitored at 506 cm^{-1} could be due to the crystal lattice of Sr–O [63]. The intensity of the carbonyl absorbance band at 1707 cm^{-1} was slightly

Table 1 EDXA (wt%) of unprinted and screen-printed nonwoven polyester fabrics at three points (A_1, A_2 and A_3) on polyester surface

Sample		C	O	Al	Sr	Eu	Dy
NPF_0		65.32	34.68	0	0	0	0
NPF_1	A_1	64.73	33.21	1.22	0.57	0.18	0.09
	A_2	64.60	33.75	1.01	0.44	0.11	0.09
	A_3	64.80	33.34	1.10	0.52	0.14	0.10
NPF_2	A_1	64.72	32.71	1.42	0.69	0.29	0.17
	A_2	65.13	32.82	1.15	0.50	0.22	0.18
	A_3	64.81	32.90	1.34	0.62	0.20	0.13
NPF_8	A_1	60.81	30.27	4.96	2.87	0.61	0.48
	A_2	60.73	30.95	4.67	2.53	0.66	0.45
	A_3	60.60	30.70	4.87	2.79	0.63	0.41
NPF_{10}	A_1	59.01	30.53	5.52	3.40	0.89	0.59
	A_2	59.64	29.96	5.34	3.65	0.85	0.57
	A_3	59.59	30.37	5.47	3.25	0.81	0.51

Table 2 XRF analysis (wt%) of screen-printed fabrics

Elements	NPF_1	NPF_2	NPF_8	NPF_{10}
Al	64.64	65.03	64.38	63.14
Sr	35.36	34.97	35.62	36.86

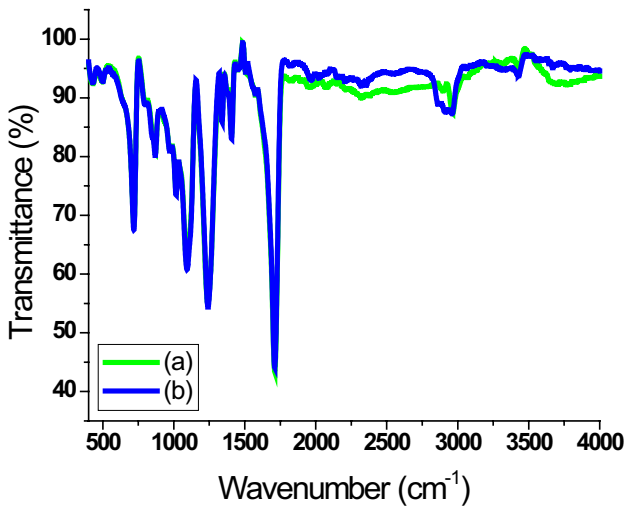

Fig. 5 FTIR spectra of nonwoven polyester fabrics; NPF_1 (**a**), and NPF_{10} (**b**)

increased with raising the phosphor ratio to verify that the phosphor aluminium coordinates as a crosslinking agent among the polyester carbonyl groups [63]. The screen-printed nonwoven polyester fabrics did not show any additional bands in comparison to unprinted fabric to indicate that the phosphor incorporation onto fabric surface did not include chemical reactions.

Colorimetric Measurements

The *K/S* and CIE systems were used to assess the sensor's capabilities. A CIE Lab is used to analyze the fabrics photochromic capabilities as well as their technical performance (photostability and fatigue resistance). L* represents the fabric lightness from the most black (0) to the most white (100), a* signifies green(−) to red(+) coloration ratios, and b* denotes the blue(−) to yellow(+) color ratio. Table 3 displays the colorimetric screening, and photochromic impacts before and after UV irradiation. All of the screen-printed polyester samples have a gray color close to the color of the original blank cloth before printing. The color data was analyzed using a high reflectance approach to get the *K/S* value. When increasing the pigment ratio, a slight increment in *K/S* was observed under daylight to designate a colorless printed layer owing to the low phosphor concentration. However, the NPF_9 and NPF_{10} polyester samples showed a white layer due to the very high phosphor concentration. Upon increasing the phosphor ratio, a significant increment in the *K/S* value was monitored under exposure to ultraviolet rays to indicate a phosphor concentration-dependent greener color. However, the polyester samples showed almost no change in *K/S* with increasing the pigment ratio from NPF_8 to NPF_{10}. Thus, the above results prove that the optimum printed samples were the photochromic NPF_2 with the green fluorescence, and the phosphorescent NPF_8 with the highest effective glow in the dark phosphor concentration. When the phosphor ratio was raised, L*, a* and b* of printed polyester samples did not vary remarkably under daylight. However, the L*, a*, and b* values showed considerable differences under ultraviolet rays with increasing the phosphor concentration. The L* values slightly decrease with increasing the phosphor concentration under daytime light, and considerably decreased under ulraviolet light. The L* values were found to considerably decrease under ultraviolet light as compared to the

Table 3 Coloration properties of printed polyesters under daylight (DL) and UV rays (UVR)

Sample	L*		a*		b*		*K/S*	
	DL	*UVR*	*DL*	*UVR*	*DL*	*UVR*	*DL*	*UVR*
NPF_0	87.85	87.51	− 5.91	− 5.92	5.11	5.23	2.33	2.28
NPF_1	87.61	87.33	− 5.75	− 6.04	5.41	5.12	2.52	2.73
NPF_2	87.34	87.06	− 5.48	− 6.15	5.83	5.09	2.72	2.95
NPF_3	86.30	86.65	− 5.21	− 6.80	6.02	4.88	2.97	3.38
NPF_4	85.06	83.12	− 4.89	− 8.78	6.19	4.30	3.10	3.90
NPF_5	84.86	80.32	− 4.63	− 11.54	6.30	3.72	3.21	4.03
NPF_6	83.40	77.54	− 4.44	− 13.46	6.53	3.21	3.44	4.54
NPF_7	82.65	74.87	− 4.27	− 16.38	6.61	2.67	3.53	5.24
NPF_8	81.90	72.64	− 4.02	− 17.63	6.74	2.16	3.75	6.37
NPF_9	81.55	71.53	− 3.88	− 18.50	6.97	1.80	3.94	6.91
NPF_{10}	81.20	71.20	− 3.76	− 18.73	7.18	1.20	4.12	7.07

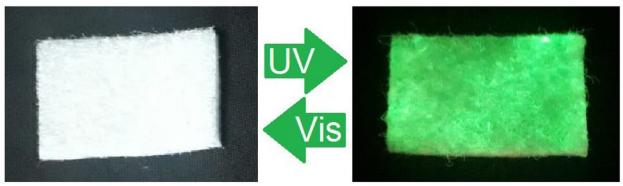

Fig. 6 Photographs of photochromic nonwoven polyester fabric (NPF_8) under daytime and ultraviolet (365 nm) lights

daytime light for the same sample. Only slight changes were observed in both − a* and + b* when raising the phosphor concentration. Under UV light, − a* and + b* noticeably increase with raising the phosphor ratio. The above results signify a color change from gray to green under UV rays.

Photochromic Properties

Screen-printing was used to apply the phosphorescent strontium aluminate pigment onto nonwoven polyester fabric (Fig. 6). On dark surfaces, the resulting bright green emission under UV-irradiation is readily visible to the human eye, making the photochromic effect more readily apparent.

Under UV light, the photochromic and fluorescent features of all of printed textiles were detected instantly and reversibly. But only garments printed with phosphor concentration up to 0.5% displayed a rapid reversibility to indicate fluorescence. Prints with phosphor content higher than 0.5% acquire afterglow effects, which results in delayed decoloration and/or reversibility to indicate long-persistent phosphorescence emission. Using excitation and emission spectral analyses, the photochromism effects were verified by strong and broad absorbance peak appeared in the visible range as depicted in Figs. 7 and 8. The excitation band increased with increasing the pigment ratio (Fig. 7). The fading emission changes were studied over time under UV irradiation (365 nm) for 50–500 s at

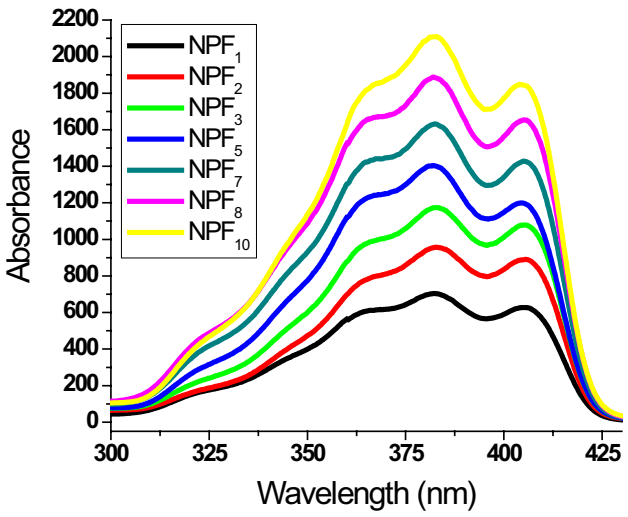

Fig. 7 Absorbance spectra of screen-printed polyester fabrics with different phosphor contents

room temperature. The emission intensity rapidly faded with time after removing the ultraviolet source (Fig. 8). Three emission peaks were detected at 418, 440 and 468 nm, and three excitation peaks were observed at 364, 382 and 404 nm. The maximum emission peak was observed at 440 nm, and the maximum excitation peak was observed at 382 nm. When exposed to UV irradiation, the printed fibers exhibit a green emission. Ultraviolet irradiation duration (50–500 s) is used to examine the emission spectra of the printed cloth (NPF_8). When the UV-irradiation period was increases, the absorbance rises.

Photostability and fatigue resistance of NPF_8 were determined by exposure to ultraviolet rays for 4 min, and placing the sample in a dark box for sixty minutes to fade back to its origin color. The irradiation/darkening practice was made several cycles, while recording the emission intensity. No differences were monitored in the emission band to indicate

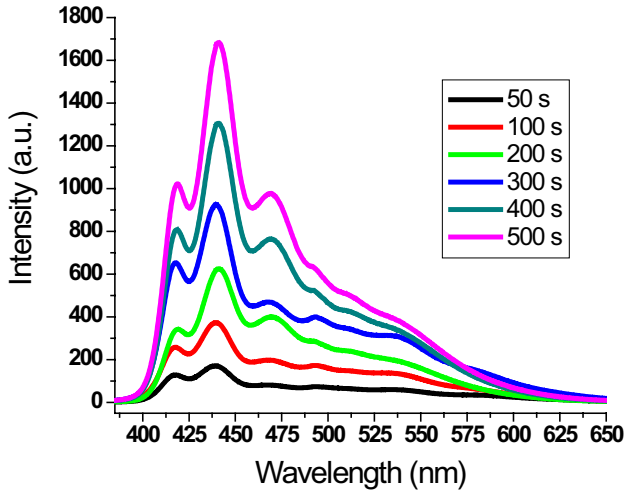

Fig. 8 Emission spectra of screen-printed polyester fabric (NPF_8) upon UV-irradiation at different periods

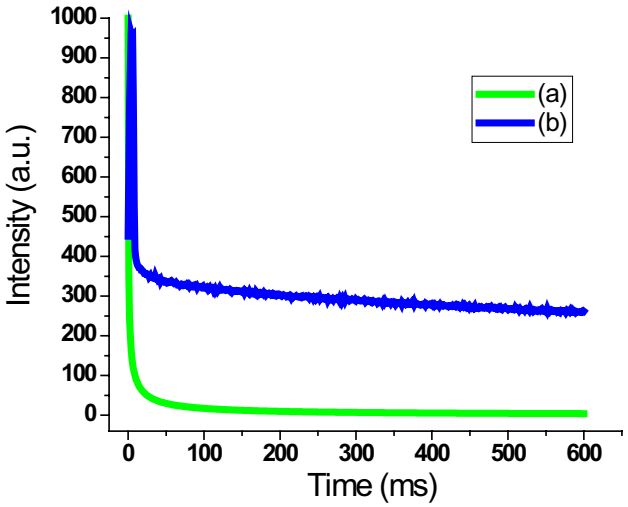

Fig. 10 Lifetime spectra of photoluminescent fabrics; NPF_3 (**a**), and NPF_{10} (**b**)

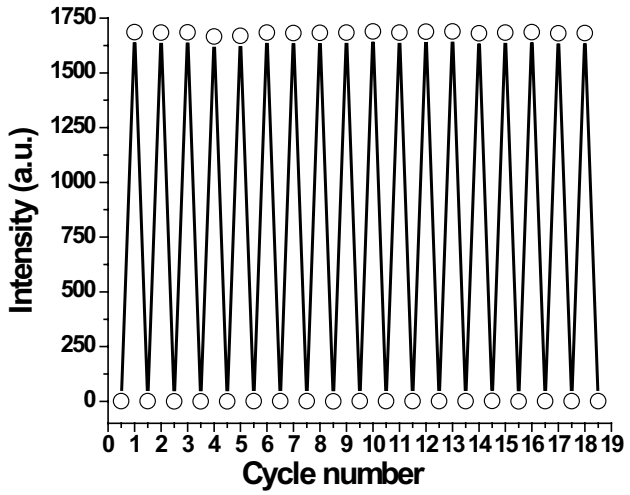

Fig. 9 Variations in emission intensity of NPF_8 at 382 nm

Table 4 Hydrophobic screening and comfort features of blank and screen-printed polyester fabrics; contact angle is represented by C.A.; slide angle is represented by S.A.; bending length is represented by B.L.; and air-permeability is represented by A.P.

Fabric	C.A. (°)	S.A. (°)	B.L. (cm)		A.P. ($cm^3\ cm^{-2}\ s^{-1}$)
			warp	*weft*	
NPF_0	107.5	12	4.23	4.46	45.83
NPF_1	108.0	12	4.37	4.50	45.67
NPF_2	109.2	12	4.54	4.72	45.24
NPF_3	112.4	12	4.65	4.81	44.85
NPF_4	115.5	11	4.77	5.91	44.53
NPF_5	120.8	11	4.90	6.05	43.60
NPF_6	126.1	10	5.10	6.13	43.82
NPF_7	130.3	9	5.21	6.22	43.61
NPF_8	131.6	8	5.32	6.37	43.33
NPF_9	131.1	8	5.53	6.53	42.90
NPF_{10}	130.7	7	5.71	6.46	42.46

that NPF_8 able to withstand repetitive irradiation/darkening cycles without fatigue (Fig. 9).

The calculated lifetimes of the screen-printed polyester fabrics ranged from 0.3347 to 488.52 ms with increasing the phosphor ratio from NPF_1 to NPF_{10}, respectively, suggesting a proportional correlation between lifetime and phosphor ratio on fabric surface (Fig. 10). The lifetime curve was non-linear against time demonstrating a rapid decrease first stage followed by slow decrease second stage. In long-persistent phosphorescent materials, Dy^{3+} and Eu^{2+} function as traps to lengthen the emission time. The polyester emission could be attributed to the Eu(II) $4f^65D^1 \leftrightarrow 4f^7$ transition [44]. Both Dy^{3+} and Eu^{2+} did not display any emission band, indicating that the lightening energy stored by Dy^{3+} was transferred to Eu^{2+}. This also verifies that Eu^{3+} was completely converted to Eu^{2+}. The excitation spectra displayed a wide spectrum (300–430 nm), allowing for absorption of a wide range of electromagnetic field.

Hydrophobicity and Comfort Features

The hydrophobicity screening of the screen-printed polyester fabrics were investigated as illustrated in Table 4. Thin film was printed onto the fibrous nonwoven polyester surface to create a rough surface by filling in the voids and gaps between fibers. Due to the hydrophobic nature and low wettability of polyester, the contact angle of NPF_0

was monitored at 108.6°. The NPF_1 exhibited an improved contact angle of 108.0°. With increasing the phosphor content, the contact angle was found to further improve from 108.0° (NPF_1) to 131.6° (NPF_8). The contact angle was then decreased from 131.6° (NPF_8) to 130.7° (NPF_{10}). The surface roughness increases with raising the phosphor content on the fabric surface [64, 65]. However, the surface roughness might be decreased at the very high phosphor concentrations due to decreasing the spaces between the phosphor particles to result in reduced contact angle [66]. Additionally, the screen-printed polyester fabrics were examined to indicate a decreased contact angle with raising the phosphor concentration. The current study can be reported as a simple, efficient and inexpensive industrial strategy to manufacture hydrophobic textiles with photochromic, long-persistent photoluminescent, ultraviolet protection and antimicrobial properties, like tents, packaging and other protecting textile fibers. The screening results of both bend length and air-permeability are shown in Table 4. Only slight differences were observed in bending length and air-permeability when increasing the phosphor concentration from NPF_0 to NPF_{10}.

Colorfastness Evaluation

The phosphor-printed nonwoven polyester fabrics displayed a good resistance to perspiration, washing, light and rubbing tests. The colorfastness properties ranged between good and excellent (Table 5). This could be attributed to the chemical binding of the phosphor nanoparticles to polyester polymer strands proving product robustness. The strong bonding of the aluminium element in the phosphor structure to the polyester oxygen atom (Al–O) can efficiently fasten the phosphor particles to polyester surface. Thus, the current strategy can be presented as an effective method to accomplish good coloration procedure with efficient colorfastness without the utilization of any further chemicals.

Antimicrobial and UV-Protection Properties

The agar counting approach [60] was employed to assess the antimicrobial activity of the printed nonwoven polyester fabrics. The antimicrobial reduction (%) generated by the screen-printed nonwoven polyester fabrics is shown in Table 5. The phosphor-free polyester sample (NPF_0) displayed a low antimicrobial activity. However, the microbial resistance of the phosphor-containing polyester textiles ranged between weak, good and very good, depending on the pigment concentration. The polyester textiles were directly evaluated for their ability to block UV rays as shown in Table 6. The blank polyester fabric exhibited low UPF value. The pigment-coated polyester textiles displayed higher UPF values than the blank fabric. The improved UV shielding

Table 6 Antimicrobial activity (antibacterial reduction %) and UPF values of blank and screen-printed polyester fabrics

Sample	*E. coli*	*S. aureus*	*C. albican*	UPF
NPF_0	18 ± 1.6	20 ± 1.0	0.00	183
NPF_1	21 ± 1.4	22 ± 1.1	0.00	202
NPF_2	23 ± 1.1	25 ± 1.5	0.00	235
NPF_3	24 ± 1.1	27 ± 1.2	0.00	270
NPF_4	27 ± 1.5	30 ± 1.4	0.00	298
NPF_5	32 ± 1.4	35 ± 1.1	0.00	352
NPF_6	36 ± 1.3	39 ± 1.6	10 ± 1.1	389
NPF_7	39 ± 1.1	44 ± 1.0	10 ± 1.0	446
NPF_8	41 ± 1.0	48 ± 1.4	10 ± 1.2	481
NPF_9	43 ± 1.2	51 ± 1.0	10 ± 1.3	506
NPF_{10}	46 ± 1.0	52 ± 1.3	10 ± 1.0	527

Table 5 Colorfastness of phosphor-printed nonwoven polyester fabrics

Fabric	Rubbing		Washing		Perspiration				Light
	Dry	Wet	Alt**	St*	Acidic		Basic		
					Alt**	St*	Alt**	St*	
NPF_1	4	4	4–5	4–5	4–5	4–5	4–5	4–5	6
NPF_2	4	4	4–5	4–5	4–5	4–5	4–5	4–5	6
NPF_3	4	4	4–5	4–5	4–5	4–5	4–5	4–5	6
NPF_4	4	4	4–5	4–5	4–5	4–5	4–5	4–5	6
NPF_5	4	4	4	4–5	4–5	4–5	4–5	4–5	6
NPF_6	4	4	4	4–5	4–5	4–5	4–5	4–5	6–7
NPF_7	4	4	4	4–5	4–5	4–5	4	4–5	6–7
NPF_8	4	3–4	4	4	4–5	4–5	4	4–5	6–7
NPF_9	4	3–4	4	4	4–5	4–5	4	4	6–7
NPF_{10}	4	3–4	4	4	4–5	4–5	4	4	6–7

*St. is cotton staining; **Alt. is color alteration

of the screen-printed polyesters can be assigned to the high ultraviolet absorbance, which could be attributed to the phosphor electronic structure making it suitable candidate for UV shielding.

Conclusion

Photochromic and long-persistent phosphorescent nonwoven polyester textile fabrics with UV protection, superhydrophobic and antimicrobial properties were industrially developed. Nonwoven polyester fibrous mat was industrially developed starting from recycled polyester waste. Nonwoven polyester fabric was screen-printed with various concentrations of phosphor nanoparticles. The printing paste is made by directly embedding the pigment doped nanoparticles into an aqueous binding agent in combination with thickening agent. After being exposed to UV, the printed polyesters displayed a color change from gray to green. This green color emission was detected at 440 nm once excited at 382 nm. In order to determine the morphology of the phosphor nanoparticles, TEM images were utilized to designate diameters of 4–11 nm. The phosphor structure was confirmed by XRD analysis to indicate a crystal size of 9 nm. The phosphor nanoscale particles must be efficiently dispersed in the printing paste by physical immobilization without aggregation to afford a transparent pigment-binder nanocomposite film onto polyester surface. Strong green fluorescence emission was monitored under UV light at lower phosphor concentrations (0.1% and 0.5%) in the printing paste. Long-persistent greenish-yellow phosphorescence was detected in the dark at higher phosphor concentrations (> 1%). Ultraviolet protection, antimicrobial and superhydrophobic properties were observed to get better with increasing the pigment concentration in the printing paste. The static contact angle was found to improve from 107.5° to 131.6°, and the slide angle decreased from 12° to 7° with increasing the pigment concentration. No compromises were detected on the garment aesthetic and comfort features after printing. Both bending length and air-permeability of the screen-printed polyesters were observed to be a little influenced by increasing the phosphor ratio. The colorfastness properties of the printed polyester fabrics ranged between good and excellent. To examine the glow in the dark property of the screen printed fabrics, we placed the ultraviolet-irradiated fabric in the dark to display an apparent greenish-yellow emission. With their excellent thermal and photostability, low-cost production, high reversibility, and fatigue resistance, the current photochromic and long-persistent photoluminescent printed samples showed potential materials for future smart clothing applications, including brand protection, smart packaging, and other security-related sectors.

Supplementary Information The online version contains supplementary material available at https://doi.org/10.1007/s10924-022-02587-y.

Acknowledgements This work was supported by the program of the Science, Technology and Innovation Funding Authority (STDF) under Grant Number 43447.

Author Contributions NGAB, TAK, HA, MSA: methodology, investigation, writing—original draft preparation; NGAB, HA, MSA: resources, data curation, writing—reviewing, formal analysis. ZW, TAK: supervision, visualization, conceptualization, formal analysis, supervision, writing-reviewing and editing.

Funding Open access funding provided by The Science, Technology & Innovation Funding Authority (STDF) in cooperation with The Egyptian Knowledge Bank (EKB). Funding was provided by Science and Technology Development Fund (Grant Number 43447).

Data Availability All data generated or analyzed during this study are included in this published article.

Declarations

Conflict of interest The authors declare that they have no conflict of interest.

Ethical Approval Not applicable.

References

1. Atav R, Ergünay U, Akkuş E (2022) Producing garment based multichromic smart sensors through dyeing cotton fabrics with chromic dyes. Cellulose 29(1):571–604
2. Khattab TA, El-Naggar ME, Pannipara M, Wageh S, Abou Taleb MF, Abu-Saied MA, El Sayed IET (2022) Green metallochromic cellulose dipstick for Fe (III) using chitosan nanoparticles and cyanidin-based natural anthocyanins red-cabbage extract. Int J Biol Macromol 202:269–277
3. Mokhtari F, Cheng Z, Raad R, Xi J, Foroughi J (2020) Piezofibers to smart textiles: a review on recent advances and future outlook for wearable technology. J Mater Chem A 8(19):9496–9522
4. Chen G, Li Y, Bick M, Chen J (2020) Smart textiles for electricity generation. Chem Rev 120(8):3668–3720
5. Khattab TA, El-Naggar ME, Al-Sehemi AG, Pannipara M, Abu-Saied MA, Taleb MFA (2022) Facile preparation strategy of photochromic dual-mode authentication nanofibers by solution

blowing spinning of cellulose nanowhiskers-supported polyacrylonitrile. Cellulose 29(11):6181–6192
6. Wu S, Fan J, Wang W, Yu D (2022) Smart screen-printed photochromic fabrics with fast color switching performance and high fatigue resistance for energy storage applications. Colloids Surf A 632:127760
7. Periyasamy AP, Vikova M, Vik M (2020) Spectral and physical properties organo-silica coated photochromic poly-ethylene terephthalate (PET) fabrics. J Text Inst 111(6):808–820
8. Seipel S, Yu J, Periyasamy AP, Viková M, Vik M, Nierstrasz VA (2018) Inkjet printing and UV-LED curing of photochromic dyes for functional and smart textile applications. RSC Adv 8(50):28395–28404
9. Hassabo AG, Mohamed AL, Khattab TA (2022) Preparation of cellulose-based electrospun fluorescent nanofibres doped with perylene encapsulated in silica nanoparticles for potential flexible electronics. Luminescence 37(1):21–27
10. Wang H, Zhang Y, Liang X, Zhang Y (2021) Smart fibers and textiles for personal health management. ACS Nano 15(8):12497–12508
11. Xing Y, Xu Y, Wu Q, Wang G, Zhu M (2021) Optoelectronic functional fibers: materials, fabrication, and application for smart textiles. J Mater Chem C 9(2):439–455
12. Sayeb S, Debbabi F, Horchani-Naifer K (2022) Investigation of photochromic pigment used for smart textile fabric. Opt Mater 128:112393
13. Guo S, Zhou S, Chen J, Guo P, Ding R, Sun H, Qian Z (2020) Photochromism and fluorescence switch of furan-containing tetraarylethene luminogens with aggregation-induced emission for photocontrolled interface-involved applications. ACS Appl Mater Interfaces 12(37):42410–42419
14. Castaing V, Giordano L, Richard C, Gourier D, Allix M, Viana B (2021) Photochromism and persistent luminescence in Ni-doped ZnGa2O4 transparent glass-ceramics: toward optical memory applications. J Phys Chem C 125(18):10110–10120
15. Kayani ABA, Kuriakose S, Monshipouri M, Khalid FA, Walia S, Sriram S, Bhaskaran M (2021) UV photochromism in transition metal oxides and hybrid materials. Small 17(32):2100621
16. El-Newehy M, Abdulhameed MM, Karami AM, El-Hamshary H (2022) Development of luminescent solution blown spun nanofibers from recycled polyester waste toward dual-mode fluorescent photochromism. J Polym Environ 30:3483–3494
17. Alhasani M, Al-Qahtani SD, Hameed A, Snari RM, Shah R, Alfi AA, El-Metwaly NM (2022) Preparation of transparent photoluminescence smart window by integration of rare-earth aluminate nanoparticles into recycled polyethylene waste. Luminescence 37(4):622–632
18. Amimoto K, Kawato T (2005) Photochromism of organic compounds in the crystal state. J Photochem Photobiol C 6(4):207–226
19. Al-Qahtani SD, Binyaseen AM, Aljuhani E, Aljohani M, Alzahrani HK, Shah R, El-Metwaly NM (2022) Production of smart nanocomposite for glass coating toward photochromic and long-persistent photoluminescent smart windows. Ceram Int 48(1):903–912
20. Mukhopadhyay A, Moorthy JN (2016) Phenomenon to functions: photochromism of diarylpyrans, spectrokinetic properties and functional materials. J Photochem Photobiol C Photochem Rev 29:73–106
21. Fan J, Bao B, Wang Z, Xu R, Wang W, Yu D (2020) High tristimulus response photochromic cotton fabrics based on spiropyran dye by thiol-ene click chemistry. Cellulose 27(1):493–510
22. Sun M, Lv J, Xu H, Zhang L, Zhong Y, Chen Z, Mao Z (2020) Smart cotton fabric screen-printed with viologen polymer: photochromic, thermochromic and ammonia sensing. Cellulose 27(5):2939–2952
23. Bao B, Fan J, Wang W, Yu D (2020) Photochromic cotton fabric prepared by spiropyran-ternimated water polyurethane coating. Fibers Polym 21(4):733–742
24. Seipel S, Yu J, Periyasamy AP, Viková M, Vik M, Nierstrasz VA (2018) Resource-efficient production of a smart textile UV sensor using photochromic dyes: characterization and optimization. Narrow and smart textiles. Springer, Cham, pp 251–257
25. Wang X, Wang W, Li Y, Wang Y (2021) Preparation of tungsten-based polyvinyl alcohol waterborne coating and development of photochromic composite fabric. Macromol Mater Eng 306(12):2100540
26. Seipel S, Yu J, Viková M, Vik M, Koldinská M, Havelka A, Nierstrasz VA (2019) Color performance, durability and handle of inkjet-printed and UV-cured photochromic textiles for multicolored applications. Fibers Polym 20(7):1424–1435
27. Mokhtar OM, Attia YA, Wassel AR, Khattab TA (2021) Production of photochromic nanocomposite film via spray-coating of rare-earth strontium aluminate for anti-counterfeit applications. Luminescence 36(8):1933–1944
28. Sun B, He Z, Hou Q, Liu Z, Cha R, Ni Y (2013) Interaction of a spirooxazine dye with latex and its photochromic efficiency on cellulosic paper. Carbohydr Polym 95(1):598–605
29. Feczkó T, Varga O, Kovács M, Vidóczy T, Voncina B (2011) Preparation and characterization of photochromic poly (methyl methacrylate) and ethyl cellulose nanocapsules containing a spirooxazine dye. J Photochem Photobiol A 222(1):293–298
30. Pardo R, Zayat M, Levy D (2011) Photochromic organic–inorganic hybrid materials. Chem Soc Rev 40(2):672–687
31. Mohammadkhani F, Montazer M, Latifi M (2020) Photo and bio activities of magnetic electrospun recycled polyester mat. J Polym Environ 28(12):3235–3243
32. Puangsansuk K, Opaprakasit M, Udomkichdecha W, Potiyaraj P (2009) Effects of saturated acids on physical properties of UPE resins prepared from recycled PET products. J Polym Environ 17(2):65–70
33. Kayaisang S, Saikrasun S, Amornsakchai T (2013) Potential use of recycled PET in comparison with liquid crystalline polyester as a dual functional additive for enhancing heat stability and reinforcement for high density polyethylene composite fibers. J Polym Environ 21(1):191–206
34. Ibarhiam SF, Alshareef HF, Alqarni SA, Shah R, Al-Qahtani SD, Almehmadi SJ, El-Metwaly NM (2022) Novel nanocomposite film developed via screen-printing of viologen polymer for anti-counterfeiting applications: photochromism, thermochromism and vapochromic. React Funct Polym 172:105186
35. Baharuddin NA, Abdul Rahman NF, Abd Rahman H, Somalu MR, Azmi MA, Raharjo J (2020) Fabrication of high-quality electrode films for solid oxide fuel cell by screen printing: a review on important processing parameters. Int J Energy Res 44(11):8296–8313
36. He P, Cao J, Ding H, Liu C, Neilson J, Li Z, Derby B (2019) Screen-printing of a highly conductive graphene ink for flexible printed electronics. ACS Appl Mater Interfaces 11(35):32225–32234
37. Chandrakar P, Baghel RN, Bisen DP, Chandra BP (2016) Persistent luminescence of CaMgSi2O6: Eu2+, Dy3 + and CaMgSi2O6: Eu2+, Ce3 + phosphors prepared using the solid-state reaction method. Luminescence 31(1):164–167
38. Zhou C, Zhan P, Zhao J, Tang X, Liu W, Jin M, Wang X (2020) Long-lasting CaAl2O4: Eu2+, Nd3 + phosphor-coupled g-C3N4 QDs composites for the round-the-clock photocatalytic methyl orange degradation. Ceram Int 46(17):27884–27891
39. Delgado T, Afshani J, Hagemann H (2019) Spectroscopic study of a single crystal of SrAl2O4: Eu2+: Dy3+. J Phys Chem C 123(14):8607–8613

40. Wan M, He K, Hong H, Wang Q, Chen Q (2018) Structure, electric, elastic and optical properties of Mn2+-doped MgAl2O4 spinel with/without an O-vacancy. Phys B Condens Matter 547:111–119
41. Jia D (2007) An enhanced long-persistent red phosphor: CaS: Eu2+, Tm3+, Ce3+. ECS Trans 2(21):1
42. Li W, Liu Y, Ai P (2010) Synthesis and luminescence properties of red long-lasting phosphor Y2O2S: Eu3+, Mg2+, Ti4 + nanoparticles. Mater Chem Phys 119(1–2):52–56
43. Abou-Melha K (2022) Preparation of photoluminescent nanocomposite ink toward dual-mode secure anti-counterfeiting stamps. Arab J Chem 15(2):103604
44. Khattab TA, Tolba E, Gaffer H, Kamel S (2021) Development of electrospun nanofibrous-walled tubes for potential production of photoluminescent endoscopes. Ind Eng Chem Res 60(28):10044–10055
45. Nance J, Sparks TD (2020) Comparison of coatings for SrAl2O4: Eu2+, Dy3 + powder in waterborne road striping paint under wet conditions. Prog Org Coat 144:105637
46. Binyaseen AM, Bayazeed A, Al-nami SY, Al-Ola KA, Alqarni SA, Abdel-Hafez SH, El-Metwaly NM (2022) Development of epoxy/rice straw-based cellulose nanowhiskers composite smart coating immobilized with rare-earth doped aluminate: photoluminescence and anticorrosion properties for sustainability. Ceram Int 48(4):4841–4850
47. Ahmed E, Maamoun D, Hassan TM, Khattab TA (2022) Development of functional glow-in-the-dark photoluminescence linen fabrics with ultraviolet sensing and shielding. Luminescence 37(8):1376–1386
48. Albrecht W, Fuchs H, Kittelmann W (eds) (2006) Nonwoven fabrics: raw materials, manufacture, applications, characteristics, testing processes. Wiley, New York
49. Zhu G, Kremenakova D, Wang Y, Militky J (2015) Air permeability of polyester nonwoven fabrics. Autex Res J 15(1):8–12
50. Maity S, Singha K (2012) Structure-property relationships of needle-punched nonwoven fabric. Front Sci 2(6):226–234
51. Al-Qahtani S, Aljuhani E, Felaly R, Alkhamis K, Alkabli J, Munshi A, El-Metwaly N (2021) Development of photoluminescent translucent wood toward photochromic smart window applications. Ind Eng Chem Res 60(23):8340–8350
52. Jiang DB, Liu X, Yuan Y, Feng L, Ji J, Wang J, Zhang YX (2020) Biotemplated top-down assembly of hybrid Ni nanoparticles/N doping carbon on diatomite for enhanced catalytic reduction of 4-nitrophenol. Chem Eng J 383:123156
53. Abumelha HM (2021) Simple production of photoluminescent polyester coating using lanthanide-doped pigment. Luminescence 36(4):1024–1031
54. Khattab TA, Elnagdi MH, Haggaga KM, Abdelrahmana AA, Aly SA (2017) Green synthesis, printing performance, and antibacterial activity of disperse dyes incorporating arylazopyrazolopyrimidines. AATCC J Res 4(4):1–8
55. Khattab TA, Haggag KM, Elnagdi MH, Abdelrahman AA, Abdelmoez Aly S (2016) Microwave-assisted synthesis of arylazoaminopyrazoles as disperse dyes for textile printing. Z Anorg Allg Chem 642(13):766–772
56. Dong WH, Liu JX, Mou XJ, Liu GS, Huang XW, Yan X, Long YZ (2020) Performance of polyvinyl pyrrolidone-isatis root antibacterial wound dressings produced in situ by handheld electrospinner. Colloids Surf B 188:110766
57. Katouah HA, El-Sayed R, El-Metwaly NM (2021) Solution blowing spinning technology and plasma-assisted oxidation-reduction process toward green development of electrically conductive cellulose nanofibers. Environ Sci Pollut Res 28(40):56363–56375
58. Deyab MA, Słota R, Bloise E, Mele G (2018) Exploring corrosion protection properties of alkyd@ lanthanide bis-phthalocyanine nanocomposite coatings. RSC Adv 8(4):1909–1916
59. Eyupoglu C, Eyupoglu S, Merdan N (2021) A multilayer perceptron artificial neural network model for estimation of ultraviolet protection properties of polyester microfiber fabric. J Text Inst 112(9):1403–1416
60. Sharma V, Ali SW (2022) A greener approach to impart multiple functionalities on polyester fabric using Schiff base of vanillin and benzyl amine. Sustain Chem Pharm 27:100645
61. Ahmed N, Ahmed R, Rafiqe M, Baig MA (2017) A comparative study of Cu–Ni alloy using LIBS, LA-TOF, EDX, and XRF. Laser Part Beams 35(1):1–9
62. Ling C, Guo L (2020) A novel, eco-friendly and durable flame-retardant cotton-based hyperbranched polyester derivative. Cellulose 27(4):2357–2368
63. El-Newehy M, El-Hamshary H, Abdulhameed MM, Tawfeek AM (2022) Immobilization of lanthanide doped aluminate phosphor onto recycled polyester toward the development of long-persistent photoluminescence smart window. Luminescence 37(4):610–621
64. Khattab TA, Mowafi S, El-Sayed H (2019) Development of mechanically durable hydrophobic lanolin/silicone rubber coating on viscose fibers. Cellulose 26(17):9361–9371
65. Kader AHA, Dacrory S, Khattab TA, Kamel S, Abou-Yousef H (2022) Hydrophobic and flame-retardant foam based on cellulose. J Polym Environ 30(6):2366–2377
66. Alzahrani HK, Munshi AM, Aldawsari AM, Keshk AA, Asghar BH, Osman HE, El-Metwaly NM (2021) Development of photoluminescent, superhydrophobic, and electrically conductive cotton fibres. Luminescence 36(4):964–976